Quasistatic rheology of foams: II. Continuous shear flow

Alexandre Kabla, Julien Scheibert, Georges Debregeas

Quasistatic rheology of foams II. Continuous shear flow

By ALEXANDRE KABLA[1], JULIEN SCHEIBERT[2] AND GEORGES DEBREGEAS[2]

[1] Division of Engineering and Applied Sciences, Harvard University, Pierce Hall, 29 Oxford Street, Cambridge, Massachusetts 02138, USA

[2]Laboratoire de Physique Statistique, Ecole Normale Supérieure, CNRS - UMR 8550, 24 Rue Lhomond, 75231 Paris Cedex 05,FRANCE

The evolution of a bidimensional foam submitted to continuous quasistatic shearing is investigated both experimentally and numerically. We extract, from the images of the sheared foam, the plastic flow profiles and the modifications of the stress field. As the imposed strain becomes larger than the yield strain, a shear-banding transition is observed leading to a spatially confined flow profile. This process is associated with a sudden increase in the temporal and spatial correlations of the plastic events. The spatial fluctuations of the static stress field is measured in different regions of the sample: the shear-band region is found to exhibit larger stress heterogeneities than the rest of the sample. This property can be associated with a decrease in the effective yield stress so that the shear-banding process can be understood as a strain-weakening instability. Furthermore, we investigate the stress fluctuations associated with the plastic rearrangements in the permanent regime of flow.

As in most non-thermal disordered systems, foams mechanical properties are history dependent: they vary with the shear sequence which has been previously applied to the sample. In the companion paper (Kabla (2006)), this behaviour was evidenced using a numerical quasistatic model of a 2D foam submitted to an oscillating strain of moderate amplitude. A fresh (unsheared) foam was found to exhibit a continuous change in its elastic modulus, normal stress difference and yield stress, as the number of applied shear cycles was increased. This evolution of the mechanical response was associated with a measurable modification of the foam structural properties: low-amplitude shearing relaxes the foam structure and produces anisotropy in the film network.

Here this effect is studied for fully developed shear flows in quasistatic regime. The numerical model described in Kabla (2006) is used and complemented by an experiment on a real, bidimensionnally confined aqueous foam in Couette geometry. We have shown, in two previous articles, that beyond a given applied strain, plastic flow localizes in a limited region of the material called shear-band (Debrégeas (2001), Kabla (2003)). In the present study, we investigate the elastic coupling between the discrete plastic events and the stress field.

In part 1, a detailed description of the experimental and numerical systems is provided. Different tests are performed to establish the existence of a quasistatic regime in the experiment, which allows for comparison with the numerical system. In part 2, the evolution of different quantities (shear stress, free energy, flow profiles) is studied during the elastic to plastic transition. In order to understand the shear-banding instability, we analyze in part 3 the mechanical effect of T1 events (the elementary plastic processes in 2D foams, figure 1 (a)) on the stress field. Based on these results, a qualitative model is

proposed that captures both the flow instability and the observed heterogeneous modification of the sample structural properties (part 4). In part 5, we investigate the dynamics of internal stress fluctuations induced by T1 events which take place in the shear-band. A statistical mechanical model is proposed that accounts for most characteristics of the stress dynamics.

1. Experiments and simulations

1.1. *Bidimensional confined foams*

3D foams are highly diffusive to light and thus hardly accessible to bulk imaging (Durian (1991), Hohler (1997)). This is why most available data on foam rheology at the bubble scale come from 2D systems. Three main experimental systems have been used: (i) Langmuir foams are formed by depositing a mono-molecular layer of amphiphilic molecules on the surface of water. The monolayer exhibits a phase transition between a dense liquid phase and a dilute gas phase (Dennin (1997), Courty (2003)). In the coexistence domain of the phase diagram, the dense and dilute regions spontaneously organize into a foam structure whose cell size is of the order of 10 microns. (ii) Rafts are made of a monolayer of soap bubbles floating at the surface of a liquid bath (Bragg (1947), Lauridsen (2002)). The raft is sometimes covered with a transparent glass plate to facilitate its observation (Abd el Kader (1999), Dollet (2005), Wang (2006)). (iii) Confined 2D foams consist of an individual layer of bubbles squeezed between two flat plates (Debrégeas (2001), Asipauskas (2003), Cantat (2004)). The bubbles diameter is adjusted so as to be larger than the distance between the plates.

In the present study, the latter configuration is used. Details of the set-up can be found in Debrégeas (2001): it is composed of an inner shearing wheel and an outer ring (of respective radius $r_0 = 71$mm and $r_1 = 122$mm) confined between two transparent plates separated by a 2mm gap. Disordered foams are obtained by bubbling nitrogen from two hoses in a controlled amount of soap solution. Here, we focus on the limit of dry (polygonal) foams with a liquid volume fraction of 1%. The mean diameter of the bubbles is of the order of 2.2mm (Fig. 1). Shearing is produced by rotating the wheel with a stepper motor while the outer ring is kept fixed. Both the wheel and the ring are tooth-shaped to avoid bubble slippage. A CCD camera, positioned above the cell allows one to monitor the foam during the experiment. The network of films is then extracted by image analysis using IDL.

This confined system has several advantages in comparison to the two other systems. First, confinement walls reduce gas diffusion between neighbouring bubbles which allows one to run experiments for about two hours without significant change in the bubbles volume. Second, this configuration prevents the dynamic coupling that occurs between the sub-phase and the foam under shear. More importantly, the confined geometry allows one to access the stress field in the material through a simple observation of the films structure. Since the area of the gas/liquid interface is fixed in the horizontal plane, the free energy F of any sub-volume $\mathcal{D}$ of the foam is given, to a constant, by the total area of the films that separates neighbouring bubbles. In the limit of an infinitely dry foam, the free energy reads:

$$F(\mathcal{D}) = 2\Gamma h \sum_{\{\text{films inside } \mathcal{D}\}} l_i \tag{1.1}$$

where Γ is the surface tension at the air-water interface and h the separation between the glass plates. The sum is performed over all the films inside the sub-volume $\mathcal{D}$, and l_i

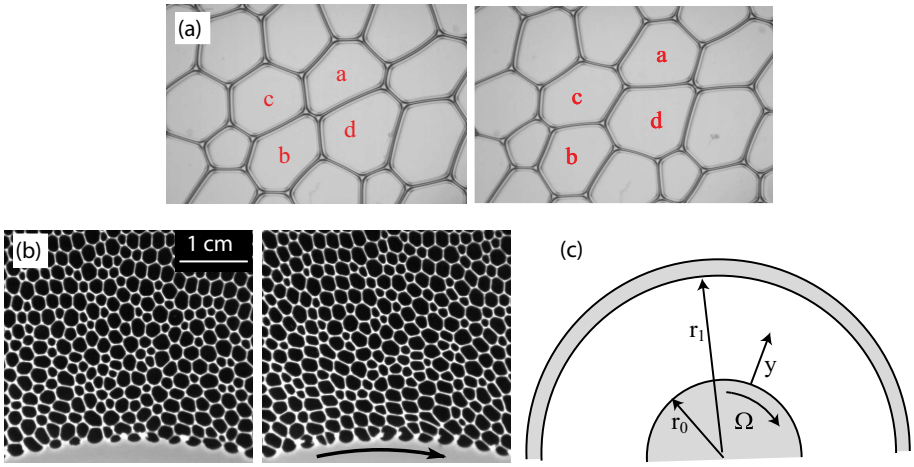

FIGURE 1. (a) Example of a T1 event in a 2D confined foam. This elementary plastic process results from the exchange of neighbours between four adjacent bubbles (noted a, b, c, and d in the pictures). (b) Two pictures of the confined 2D foam: (left) initial (unsheared) foam (right) foam under strain. (c) Definition of the different geometrical and kinetic parameters.

are the horizontal lengths of the films. From this expression, we introduce the line tension γ defined as: $\gamma = 2\Gamma h$. Consistently, the internal capillary stress in the confinement plane can also be extracted from the projected film network (Kraynik (2003)):

$$\sigma_{xy}(\mathcal{D}) = \frac{\gamma}{A(\mathcal{D})} \cdot \sum_{\{\text{films inside } \mathcal{D}\}} \frac{l_{i,x} \cdot l_{i,y}}{l_i} \tag{1.2}$$

It should be noted that these two relationships are not valid for rafts in which bubbles can deform in the vertical direction to accommodate horizontal stresses.

1.2. *The quasistatic regime of flow*

The main limitation of this experimental system is due to the viscous stress exerted by the confining walls on the foam upon shearing. The motion of the soap films induces liquid flows in the plateau borders that connect the films to the plates. This yields a net viscous force than can overcome the internal friction between bubbles (Cantat (2004)). As a model of foam bulk rheology, this system is thus only valuable in the limit of quasistatic flow. This regime is expected when the shearing time-scale $\tau_{shear} = \dot{\varepsilon}^{-1}$ is shorter than the time-scale for stress relaxation τ_{relax} associated with a plastic event†. The flow then consists of a series of elastic charges interrupted by stress drops associated with the (rapid) plastic yieldings (Pratt (2003)). During the charge periods, the foam is in static equilibrium whereas all dissipative processes take place during the fast rearrangement events.

Measuring the time τ_{relax} is not straightforward. The duration of the local film swapping process itself can be evaluated to $\tau_{T1} \sim 0.1s$ by direct visualization. In a 3D foam, the resulting deformation of the material propagates outwards via rapid elastic waves, so that τ_{relax} is in the same range. In a confined foam system, however, the elastic waves are overdamped by the friction with the confining walls so that the equilibration time following a T1 event grows linearly with the system size. In the present case, this yields

† In order to be consistent with the companion paper, and to avoid any confusion with the notation γ for the surface tension, the shear strain will be systematically noted ϵ.

an estimation of the relaxation time $\tau_{relax} \sim 10 \cdot \tau_{T1} \sim 1s$. It should be noticed that, due to shear-banding, the maximal local shear rate $\dot{\varepsilon}_{max}$ is much larger than the mean shear rate controlled by the wheel rotation rate.

In order to determine the limiting rotation rate Ω for which the flow is quasistatic, several tests are carried out. For different value of Ω, we monitor the bubbles displacements during the time period $\tau_0 = D/(r_0\Omega)$ needed for the wheel edge to move over one mean bubble diameter D. These kinematic measurements are performed in the permanent regime of flow which is found to be reached after the wheel has been rotated one full turn. Averages are calculated over the time and the angular coordinate. We thus extract the average displacement $u_{\parallel}(y)$ in the direction of the flow and the standard deviation of the radial displacement $\sqrt{\langle u_{\perp}(y)^2 \rangle}$ as a function of the distance y from the edge. Both quantities are scaled by the bubble diameter D.

Figure 2(a) shows the resulting profiles for two different rotation rates $\Omega = 2.9 \cdot 10^{-3}$ and $5.8 \cdot 10^{-3} rad \cdot s^{-1}$. The plastic flow is mostly confined in a small region - the so-called shear-band - in the vicinity of the wheel edge. The average flow profile $u_{\parallel}(y)$ exhibits an exponential decay from the wheel edge toward the outer ring. The decay length is approximately one bubble diameter (Debrégeas (2001)) so that the maximum local shear-rate is of the order of $\dot{\varepsilon}_{max} \sim \Omega r_0/D$.

Although the mean displacement in the shear direction is barely measurable beyond the fifth row of bubbles, the standard deviation of the transverse displacements remains large all across the gap. These latter are a signature of the long-range elastic deformations induced by plastic events in the shear bands (see part 5). The similarity of the curves for the two different rotation rates establishes that the dynamic is quasistatic. In this regime, the only relevant parameter is the total imposed strain and not the shear rate. From this point forward, all the experiments are performed at the same rotation rate which is set at $\Omega = 2.9 \cdot 10^{-3} rad \cdot s^{-1}$, corresponding to $\dot{\varepsilon}_{max} = 0.1 s^{-1}$ †.

Further proof of the quasistaticity of the flow at this shear-rate is obtained through a mechanical approach. In order to demonstrate that the viscous stress due to the confining wall is negligible, as expected in quasistatic flow, we check that the only contribution to the internal stress is due to surface tension. Using equation 1.2, the average shear stress profile along the radial direction is measured (Figure 2(b)). It appears to follow the expected decay for a cylindrical Couette geometry:

$$\sigma_{xy}(y) = \sigma_{xy}(y = 0) \cdot \left(\frac{r_0}{r_0 + y} \right)^2 \tag{1.3}$$

This result confirms that the foam is, at any time, in static mechanical equilibrium‡.

† It should be noted that, for larger rotation rates, a rapid decrease in the amplitude of the transverse fluctuations is observed, although the shear profile remains mainly unchanged. This indicates that the independence of the average shear profile with the imposed shear rate is not a sufficient criterium to establish the quasistaticity of the flow.

‡ At this point, we wish to comment on a recent result of Wang *et al.* (Wang (2006)) who showed that different quasistatic flow profiles could be obtained with bubbles rafts depending on the presence or absence of a covering plate. The authors claim that this result establishes that the viscous friction with the confining plate is involved in the shear-banding process. This explanation seems improper: if the flows are indeed quasistatic, viscous stresses are, by definition, irrelevant.

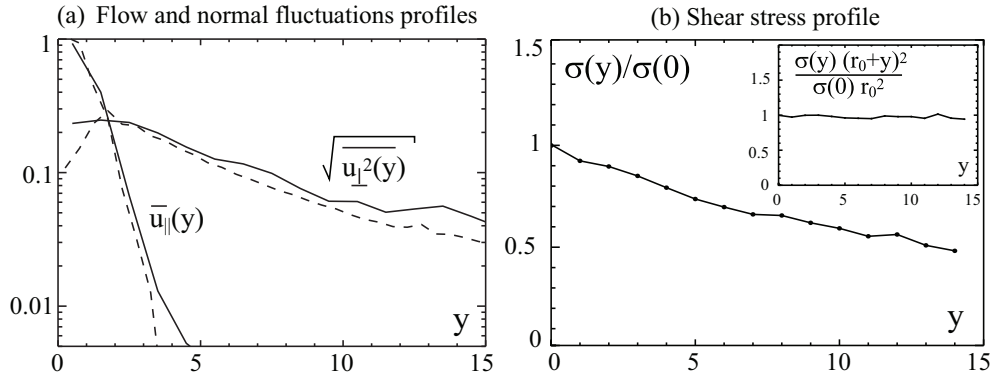

FIGURE 2. (a) Shear velocity profiles $u_\parallel(y)$ and transverse fluctuations profiles $\sqrt{\langle u_\perp(y)^2\rangle}$ for different rotation rates $\Omega = 2.9 \cdot 10^{-3} rad \cdot s^{-1}$ (solid line) and $\Omega = 5.8 \cdot 10^{-3} rad \cdot s^{-1}$ (dashed line) (data from the experiment). These measurements are obtained by averaging displacements over the time and the angular coordinate. The radial displacements are obtained by tracking the bubbles over a time τ_0 corresponding to a displacement of the inner wheel equal to a bubble diameter D. (b) Shear stress profile as a function of the distance from the inner wall. The inset demonstrates that this profile is consistent with the expected stress decay in Couette geometry (equation 1.3).

1.3. *Numerical model*

From equation 1.1, it appears that the static equilibrium configuration of the foam corresponds to a minimum of the total length of the (projected) 2D film network, with the constraint of fixed bubbles volume. This is precisely the basis of the quasistatic simulation, described in the companion paper, which therefore provides a realistic numerical counterpart to this set-up.

In Kabla (2003), we showed that the numerical foam exhibits a shear-banding instability whose characteristics are similar to those observed in the experimental system (Debrégeas (2001)). The comparison of these two results demonstrates that the shear-banding process is not a mere consequence of the mean shear stress decay associated with the Couette geometry (see formula 1.3). Indeed, the numerical simulations are performed in plane parallel geometry for which the shear stress is homogeneous across the gap.

In the present article, we combine the two systems to study in detail the transition to shear-banding as well as the dynamics of local stress fluctuations in the permanent regime of flow. The numerical procedure for the evolution of the foam under shear, and the definition of the different quantities monitored, are similar to those described in the companion paper (Kabla (2006)). The dimension of the numerical foam in the shear direction is increased in order to limit non-physical correlations induced by periodic symmetry. The numerical foam dimension is thus 40x16 bubbles. When possible, results from both the experiment and the simulation are presented. However, due to the limited resolution of the experiment, some measurements can only be obtained with the numerical system.

2. Transition to shear banding

To examine the transition to shear-banding, an experiment is performed in which the wheel is first rotated counter-clockwise one full turn. The evolution of the foam is then monitored as the wheel is rotated backwards. Figure 3 shows the modification of the displacement profiles in the shear direction $u_\parallel(y)$ as the imposed deformation is

increased from 0 to 2, as well as the corresponding profile in the permanent regime. All distances are scaled with the displacement u_0 of the wheel edge during the same period. For small imposed strain ($\epsilon \sim 0.25$), the foam deforms almost elastically (very few T1 events occur). The corresponding profile is consistent with what is expected for a linear elastic deformation in Couette geometry:

$$u_{\parallel}(y) = u_0 \cdot \frac{(y+r_0)/r_1 - r_1/(y+r_0)}{r_0/r_1 - r_1/r_0} \tag{2.1}$$

where r_0 and r_1 are respectively the inner and outer diameters. Beyond $\epsilon \sim 0.25$, strain begins to localize in a shear-band. For $\epsilon \geq 1$, The flow has reached its permanent regime and the flow profile exhibits an exponential decay: $u_{\parallel}(y) = u_0 \ \exp(-y/\lambda)$, with $\lambda \sim 1.2$.

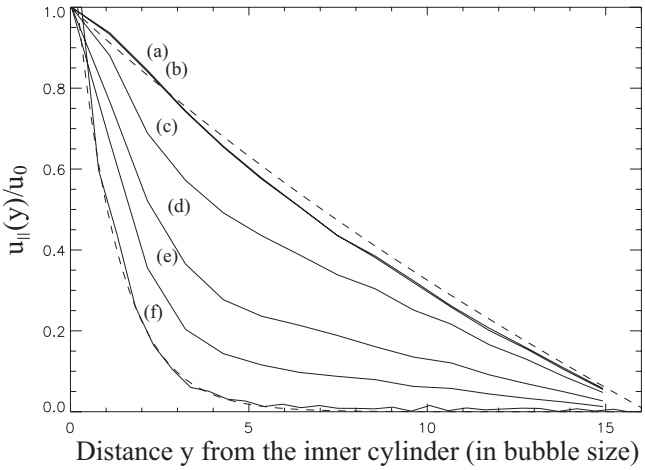

FIGURE 3. Transition from the purely elastic response to localized flow (experiment). The averaged displacement profile is plotted for different imposed deformations: (a) $0 < \overline{\varepsilon} < 0.125$, (b) $0 < \overline{\varepsilon} < 0.25$, (c) $0 < \overline{\varepsilon} < 0.5$, (d) $0 < \overline{\varepsilon} < 1$, (e) $0 < \overline{\varepsilon} < 0.2$, (f) $2 < \overline{\varepsilon} < 8$. The curves (a) and (b), which almost overlap, correspond to the expected response of an elastic material (dashed line $u_{\parallel}(y) = u_0((y+r_0)/r_2 - r_2/(y+r_0))/(r_1/r_2 - r_2/r_1)$ with r_2/r=1.5). The profile in permanent regime (f) is fitted by an exponential: $u(y) = u_0 \ \exp(-y/1.2)$.

In the experiment, the introduction of the foam in the gap involves the shearing of the material in a poorly controlled way. The numerical simulation is therefore more adequate to probe the transient regime of shear which strongly depends on the shear history of the sample. Figure 4 shows, as a function of the wall displacement noted d, the evolution of the mean shear stress, the energy of the foam (total film length), and the position of the T1 events across the gap. The line tension is set at 1, and the foam dimensions are set at L_xxL_y = 2.5x1; the parameter d is thus numerically equivalent to the total applied strain $\overline{\varepsilon} = d/L_y$. For $\overline{\varepsilon} < 1$, an elastic deformation of the material is observed, interrupted by a small number of T1 events uniformly distributed across the gap. For $\overline{\varepsilon} \sim 1$, shear-banding occurs: most of the T1 events gather in a narrow region close to one of the confining walls. The sharp transition is associated with an overshoot of the shear stress and the appearance of large avalanches of rearrangements, as evidenced by the increase of the drops amplitude in the shear stress and energy curves (figure 4(a) and 4(b)).

As the foam is sheared, it experiences a series of plastic events that modify its topological structure. Each metastable configuration is entirely characterized by the relative positions of the bubbles. We showed in the companion paper that this trajectory in the

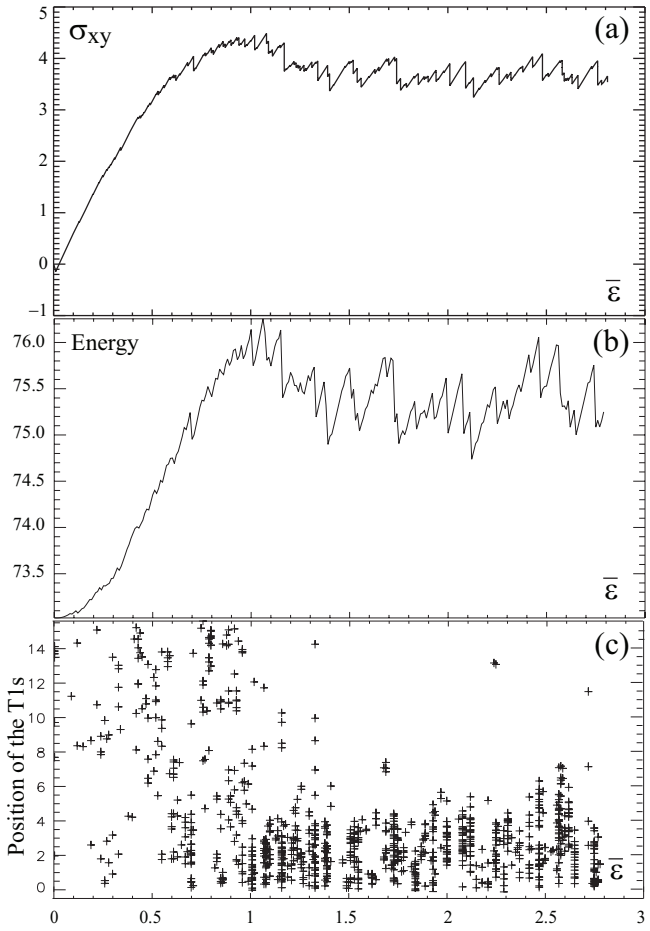

FIGURE 4. Evolutions of (a) the shear stress, (b) the free (line-length) energy and (c) the positions of the T1 events within the gap as a function of the applied strain $\bar{\epsilon}$ (data from the simulation).

configuration space can be associated with a path in an energy landscape. After each T1 event, the system falls into a new energy basin which is defined as the energy versus strain relation of the given structure.

For each value of the total imposed strain $\bar{\varepsilon}$, this quadratic function can be numerically obtained the following the method detailed in Kabla (2006): after an imposed strain $\bar{\varepsilon}$, the possibility for T1 events to occur is forbidden in the simulation so that only the elastic response of the structure is probed. The line-length energy of the foam $E(\varepsilon')$ is then monitored as a function of the strain ε' and the resulting curve is fitted using the following relation:

$$E_{elast}(\varepsilon') = E_0(\bar{\varepsilon}) + \frac{A\mu(\bar{\varepsilon})}{2}\,(\varepsilon' - \varepsilon_{plast}(\bar{\varepsilon}))^2 \tag{2.2}$$

where A is the total area of the foam. This allows one to extract, for each configuration reached after an imposed strain $\bar{\varepsilon}$, several parameters that define the energy basin: E_0 is the minimum energy of the structure, μ is the shear modulus and ϵ_{plast} is the value of the shear strain (or equivalently the position of the wall) for which the foam energy is

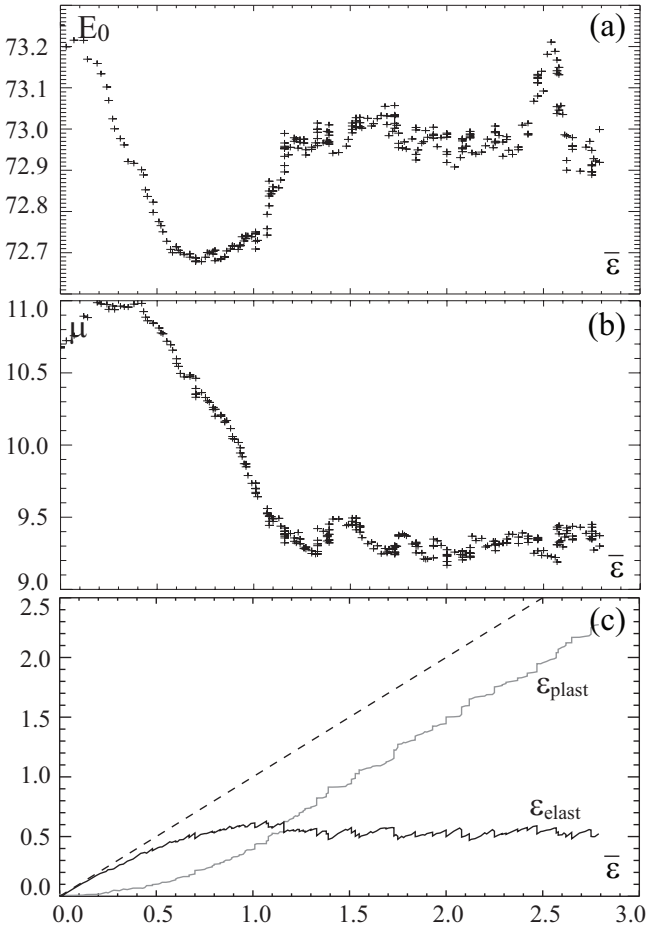

FIGURE 5. Evolutions of (a) the structural energy E_0, (b) the shear modulus, and (c) the plastically relaxed and elastically stored strain components as a function of the imposed strain (data from the simulation). In graph (c), the dotted line is the sum of the two components of strain which, by definition, is equal to the imposed strain.

minimum. The latter can be viewed as the amount of strain that has been irreversibly released through the successive plastic events that have occurred since the shear started. The imposed strain can thus be decomposed into an irreversible (plastic) and a stored (elastic) component: $\bar{\varepsilon} = \varepsilon_{elast} + \varepsilon_{plast}$.

Figure 5 shows the evolution of these different parameters as a function of the imposed strain $\bar{\varepsilon}$. In agreement with the findings of the companion paper, E_0 and μ are found to decrease with the strain for $\bar{\varepsilon} < 0.5$. In this transient regime, ε_{plast} remains almost constant which indicates that the initial T1 events relax the structure but do not significantly release the shear strain. As the system enters the localized regime, a significant increase of E_0 is observed whereas μ remains unchanged. The plastic component of the strain ε_{plast} becomes greater whereas the elastic part reaches a constant value. In the permanent regime, the T1 events mainly release the imposed strain.

2.1. *Discussion*

In the numerical simulation, although the imposed stress is uniform, the flow is highly asymmetrical. As already pointed out by previous studies (Varnik (2003), Kabla (2003)),

this observation hampers the possibility to describe the foam mechanical response using a rheological equation such as $\sigma = f(\dot{\epsilon})$. In particular, the Hershel-Buckley model, $\sigma = \sigma_0 + \mu\dot{\epsilon}^n$, which is commonly used for aqueous foams, is expected to fail in the limit of $\dot{\epsilon} = 0$. This has been recently established by Rodts *et al.* using MRI imaging of 3D foams sheared in a Couette cell (Rodts (2005)). The authors observe a discontinuous drop of the shear-rate measured across the gap, from $\dot{\epsilon}_c = 10s^{-1}$ to 0. The width of the transition zone, which is below the MRI resolution, is believed to be of the order of a few bubble diameters.

This observation can be understood by noting that $\dot{\epsilon}_c^{-1} = 0.1s$ is of the order of the duration of a T1 event. When the average strain rate falls below this critical value, the flow becomes intermittent: the local instantaneous strain rate is either 0 in the absence of T1 process, or $\dot{\epsilon}_c = 1/\tau_{T1}$ when a T1 occurs. In this regime, the long-range elastic stress that couples the different regions of the material becomes dominant over local viscous stress and allows for spatially heterogeneous flow to develop. In the case of Rodts' experiment, as well as in our system, this leads to an abrupt decay of the plastic strain rate over a distance of a few bubble diameters.

In order to understand the spatial and temporal statistics of the plastic processes in the intermittent regime, one needs to probe the elastic effect of the plastic events on the entire material. This is done in the next chapter using the results of the numerical simulation which, in contrast to the experiment, provides a sufficient resolution for such a study.

3. The short-time scale: T1 and avalanche

3.1. *Elastic effect of a T1*

The stress field in the foam can be evaluated by extrapolating the expression 1.2 to small sub-regions (in practice down to the bubble size). By comparing the equilibrated structures of the foam before and after a rearrangement, one can extract the local displacement and shear stress variation induced by the event on each bubble. Figure 6 displays the resulting fields for a T1 event located either in the middle of the foam or close to one of the walls. In order to improve the spatial resolution of the measurements, the data are averaged over one hundred T1 events located at the same distance from the wall.

We first focus on the line-averaged (along the shear direction x) characteristics of the propagator. The average shear stress relaxation is found to be identical for each line as imposed by the constraint of mechanical equilibrium. The graphs 7 (a) and (b) show the displacement profiles: to first order, a T1 event is equivalent to a shift running along the line of the T1 event. The upper part of the material "slides" with respect to the lower part over a length δd_{T1}. In each sliding block, the displacement profile is linear and the slope defines a shear strain $\delta\varepsilon_{T1} = \frac{\delta d_{T1}}{L_y}$ where L_y is the gap width.

Due to the foam polydispersity, a 30% dispersion in the these quantities is observed. However, a scaling of the mean length δd_{T1} can be estimated by considering that the bubbles involved in the T1 move by a distance of order D, whereas the L_x/D bubbles in the rest of the line do not rearrange (L_x is the size of the foam in the x direction). Thus the average sliding distance δd_{T1} is expected to write:

$$\delta d_{T1} \simeq D \cdot \frac{D}{L_x} \tag{3.1}$$

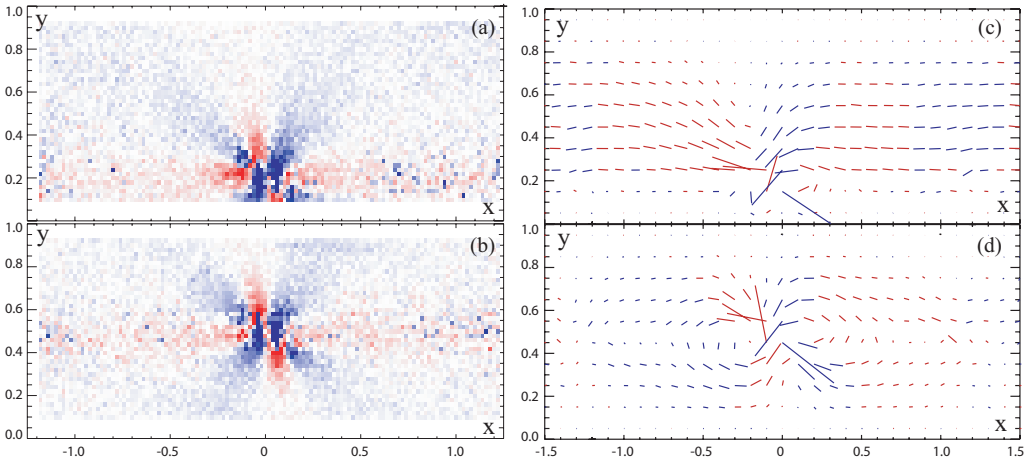

FIGURE 6. Shear stress variation (a-b) and displacement (c-d) fields induced by a T1 event, respectively located close to the wall and in the middle of the gap. These simulation data have been obtained by averaging 100 different T1 events located at the same distance from the wall. In figure (a) and (b), the blue colour corresponds to a stress decrease (with respect to the imposed stress), the red colour to a stress increase.

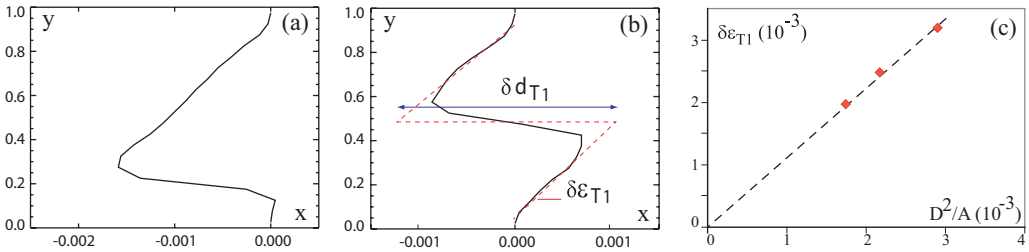

FIGURE 7. (a) and (b): the deformation profiles (x-averaged displacement) induced by a T1 event located (a) near the wall and (b) in the middle of the gap. δd_{T1} is the mean sliding distance, and $\delta\varepsilon_{T1}$ the corresponding elementary strain release induced by the T1 event. Due to the foam polydispersity, a 30% dispersion in the these quantities is observed.(c): dependence of $\delta\varepsilon_{T1}$ with the system size (D is the mean bubble diameter and A is the foam area). Each data point corresponds to an average over 100 T1 events.

The elastic deformation released by the T1 event thus writes:

$$\delta\epsilon_{T1} = \frac{\delta d_{T1}}{L_y} = \frac{D^2}{A} \tag{3.2}$$

where A is the total area of the foam. These two relations are successfully confirmed by varying the system size (figure 7(c)). Recent analytical results of Picard *et al.* (Picard (2004)) show that this propagator corresponds to the response of a 2D elastic material to an elementary force quadrupole. It should be stressed, however, that the T1 propagator is slightly asymmetrical: this might be due to the elastic anisotropy of the foam induced by the shearing.

Having identified the result of a single T1 event, the cumulative effect of a series of these plastic events on the evolution of the stress field can now be examined. As previously, we consider a system of size (Lx, Ly), sheared along the x direction, with an imposed shear rate $\dot{\bar{\varepsilon}}$ in quasistatic regime. We denote $u_{\|}(y,t)$ the displacement in the x direction

at a distance y from the wall, averaged over the shear direction. The associated strain $\varepsilon(y,t) = du_{\parallel}/dy$ is decomposed into a (stored) elastic term $\varepsilon_{elast}(y,t)$ and a plastic term $\varepsilon_{plast}(y,t)$:

$$\varepsilon(y,t) = \varepsilon_{elast}(y,t) + \varepsilon_{plast}(y,t) \tag{3.3}$$

The function $\omega(y,t)$ is defined as the density function of T1 events occurring at a time t and a height y in the foam:

$$\omega(y,t) = \sum_{\text{T1 } i} \delta(y - y_i) \cdot \delta(t - t_i) \tag{3.4}$$

When a rearrangement occurs at a location y_{T1}, it increases the plastic strain by a quantity δd_{T1} at $y = y_{T1}$, and elastically relaxes the entire system by a strain amplitude $\delta\epsilon_{T1} = \frac{\delta d_{T1}}{L_y}$. One can thus write:

$$\frac{\partial\, \varepsilon_{elast}(y,t)}{\partial t} = \dot{\bar{\varepsilon}} - \delta\varepsilon_{T1} \cdot \int_y \omega(y',t)dy' \tag{3.5}$$

$$\frac{\partial\, \varepsilon_{plast}(y,t)}{\partial t} = \omega(y,t) \cdot \delta d_{T1} \tag{3.6}$$

The integral in Equation 3.5 is a direct consequence of the long range elastic effect of T1 events. The strain evolution at any location in the foam depends on all the rearrangements occurring in the system. Moreover, $\varepsilon_{elast}(y,t)$ does not depend on y; as the local shear stress is uniform in all the lines, the elastically stored deformation also remains uniform. These equations yield a relationship between the statistics of the plastic events and the flow profile $v(y) = du_{\parallel}/dt$ in permanent regime:

$$\frac{dv(y)}{dy} = \left\langle \frac{\partial\, \varepsilon(y,t)}{\partial t} \right\rangle_t = \underbrace{\left\langle \frac{\partial\, \varepsilon_{elast}(y,t)}{\partial t} \right\rangle_t}_{=0} + \left\langle \frac{\partial\, \varepsilon_{plast}(y,t)}{\partial t} \right\rangle_t \tag{3.7}$$

$$\Rightarrow \quad \frac{dv(y)}{dy} = \langle \omega(y,t) \rangle_t \cdot \delta d_{T1} \tag{3.8}$$

This relationship is demonstrated on figure 8 which displays both the gradient of the flow profile and the histogram of the T1 event locations in permanent regime. The elastic behavior of the foam therefore couples local plastic events and global shear stress relaxation, allowing for the existence of heterogeneous flow profiles. This approach shows that any flow profile is consistent with the mechanical equilibrium condition, as each T1 event produces the same stress relaxation in each line, regardless of its location in the gap. Therefore, this line-averaged description appears inadequate to address the question of the shear-banding instability and further examination into the origins of the spatial correlations between T1 events is needed.

3.2. *From a T1 event to the avalanche*

When a T1 event occurs, it generally triggers an avalanche of events that take place in the neighbouring region. Figure 9 (a) shows the distribution of avalanche sizes measured in numbers of T1 events. A power-law decay of the avalanche size distribution is observed, with an exponent -1.5 consistent with numerical studies on elastic disordered systems (Chen (1991), Okuzono (1995)). As shown in figure 9(b), the energy released during the

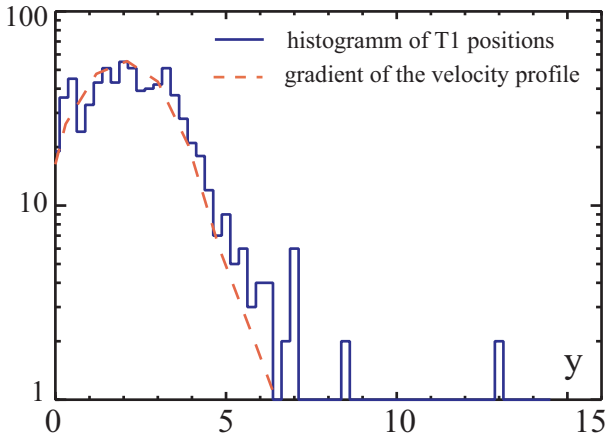

FIGURE 8. Gradient of the flow profile and frequency of the T1 events for each line (simulation). The coordinate y is expressed in bubble diameter D.

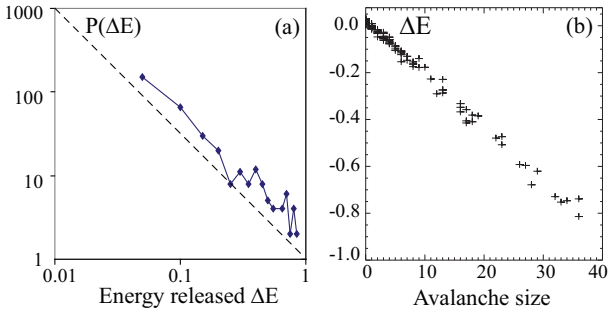

FIGURE 9. (a) Distribution of the elastic energy released by the avalanches of plastic events (b) Released energy as a function of the number of T1 events involved. These results come from the simulation data in permanent regime.

avalanche is a linear function of the avalanche size: each rearrangement releases a given amount of energy (or shear stress) which numerically coincides with $A \cdot \delta\epsilon_{T_1} \cdot \overline{\sigma_{xy}}$.

The avalanches appear to develop preferentially along shear lines, as illustrated in figure 10. This trend can be understood from the observation of the pattern displayed in figure 6, which shows that the shear stress variation field induced by a T1 event is highly anisotropic. Although the shear stress is globally relaxed, it is increased in some regions, in particular in the line where the T1 event occurred. This increase is likely to trigger further T1 events in the same line and can lead cumulatively to a complete "unzipping" of the line as illustrated in figure 10.

Due to the disordered nature of the foam, the collective reorganization of the bubbles in the shear-band is very different from the standard dislocation motion that controls plasticity in crystalline 2D foams (Bragg (1947)). Figure 10(c) shows the location along the shear band of the successive rearrangements during the two avalanches. Although consecutive T1 events are often nearby, after 3 to 4 rearrangements, the location of the plastic events typically moves to another part of the shear band.

We quantitatively analyse this process during the permanent regime by measuring the spatial correlations of the rearrangements along the flow direction. Figure 11(a) shows the coordinate x_i of the i^{th} T1 event as a function of i. The shear-band develops af-

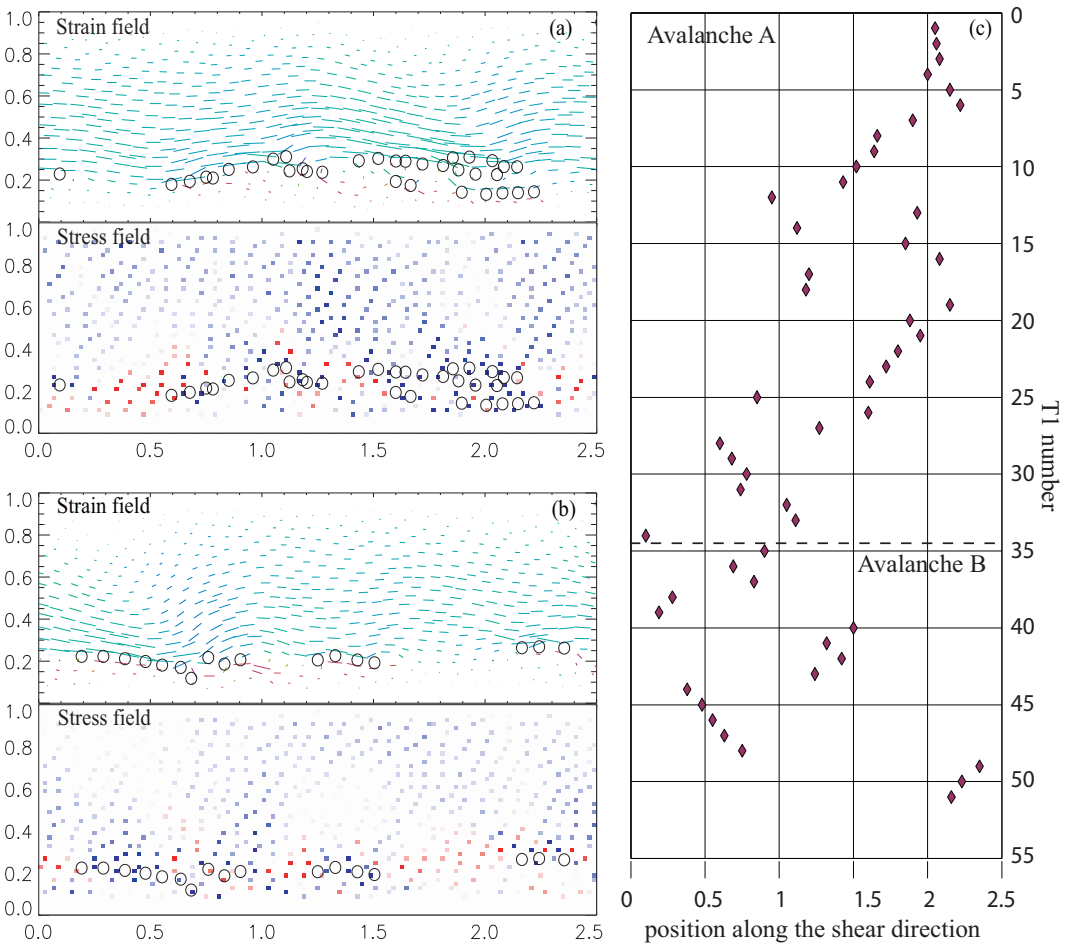

FIGURE 10. (a-b) Description of two successive avalanches in permanent regime (numerical simulation). For each one, the displacement and stress fields, resulting from the T1 cascade, are displayed. The circles corresponds to the location of the T1 events that constitute the avalanche. (c) x coordinate (along the shear-band) of the T1 events in chronological order for the 2 avalanches described on the left. The dotted line indicates the limit between the two avalanches. This graph illustrates that the second avalanche involves T1 events preferentially in the region that have not plastically yielded previously. An animation showing the complete sequence of these two avalanches is available online: `http://tel.ccsd.cnrs.fr/docs/00/04/56/98/HTML/Ava97.gif` & `http://tel.ccsd.cnrs.fr/docs/00/04/56/98/HTML/Ava98.gif`

ter 300 rearrangements (dashed-line). From this point forward, the probability function $P_k(\Delta x) = \sum_{i=1}^{N} \delta\left(x_{i+k} - x_i - \Delta x\right)/N$ is computed (P_k represents the probability for two rearrangements separated by $k-1$ events in the sequence to be located at a distance Δx from each other). The two large peaks of P_1 at $\Delta x = \pm D$ in Figure 11(b) demonstrates the existence of strong spatial correlations between successive rearrangements. However, this correlation vanishes after about 3 rearrangements as indicated by figure 11(c) which shows the decay of the spatial correlation as a function of the difference in the indexes of the two T1 events.

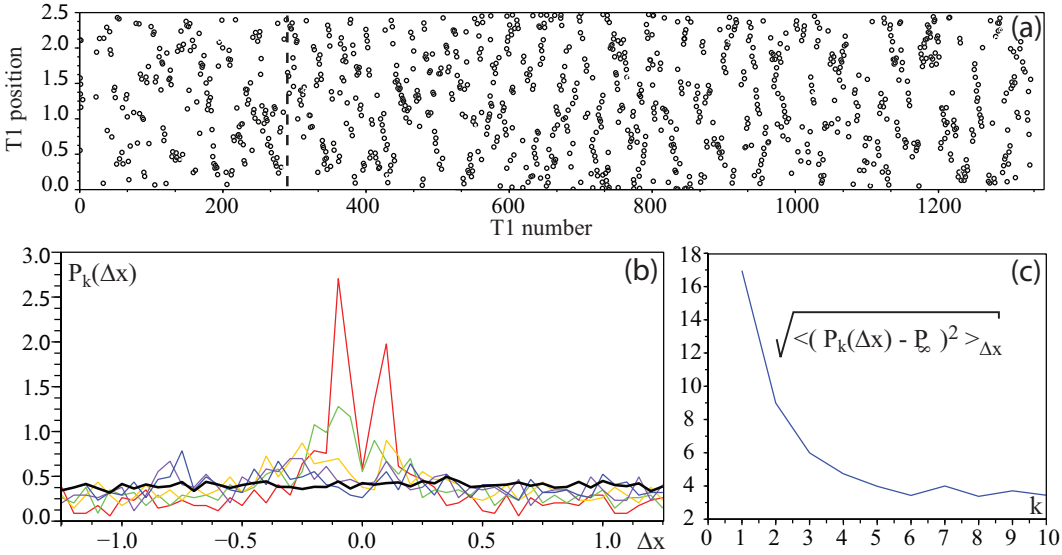

FIGURE 11. (a) Position x_i of the rearrangements along the shear direction, as a function of the index i of the rearrangement in the sequence (i is the total number of rearrangements that have occurred since the beginning of the simulation). (b) Probability function $P_k(\Delta x)$ (see text) for different values of k: 1 (red), 2 (green), 3 (yellow), 4 (violet), 5 (blue). The black curve corresponds to $\sum_{20\leq k<30} P_k(\Delta x)/10$. At long time scale $P_k(\Delta x)$ is constant, with a value $P_\infty = 1/L_y$. (c) Deviation from the uncorrelated statistics, as a function of the difference k in the indexes of the two T1 events.

4. The shear-banding instability

The previous section showed that the peculiar form of the stress propagator associated with a T1 event can account for the appearance of fracture-like processes orientated along the shear direction. This is a first step toward the understanding of the shear-banding instability. However, it does not explain why successive avalanches take place in the same region of the foam so that the shear-band is stable in the long run. In the experiment, this could be due to the decay of the mean shear stress across the gap inherent to the Couette geometry, which would maintain the shear band in the region of higher stress near the inner cylinder. However, the numerical study establishes that the same process occurs in plane-parallel shearing geometry in which the shear stress is homogeneous across the gap.

The stability of the shear band over time suggests that the shear-banding process is associated with the development of structural heterogeneities which remain permanently imprinted in the foam. To test this hypothesis, we attempt to identify local quantities that may differ in the shear-band as compared with the rest of the material. In contrast with many studies based on topological measurements (the so called μ_2 parameter for instance, Weaire (1983), Weaire (1997), Abd el Kader (1999)), here we focus on energetic and mechanical parameters. This approach aims at offering a more generic framework which may be extended to other disordered systems.

4.1. *Spatial fluctuations of the static stress field*

The disordered nature of the foam structure results in spatial heterogeneities of the static stress field. To characterize these fluctuations, we evaluate, for each bubble of index i at time t, the quantity:

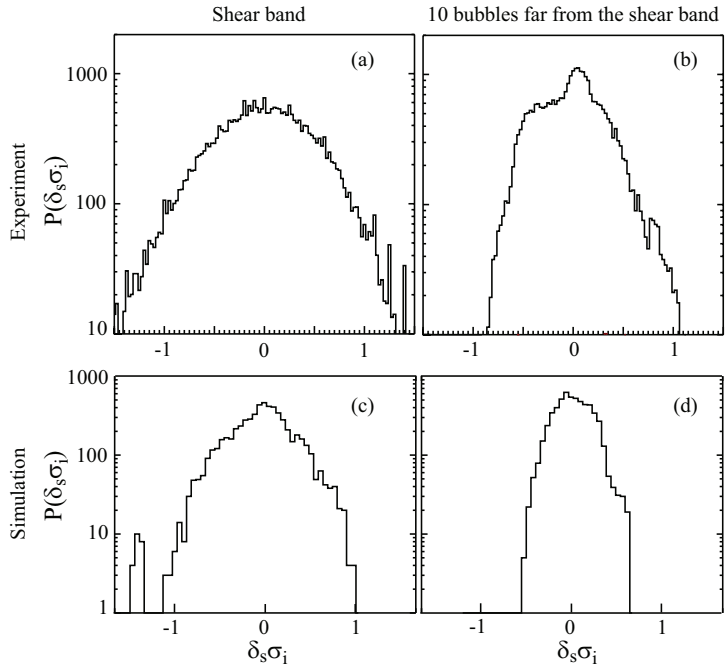

FIGURE 12. Distribution of the bubble shear stress $\delta_s\sigma(i)$ for the experiment (a and b) and the simulation (c and d), in permanent regime. Two different regions are analysed: the shear band, and a region located 10 bubble diameters away from the shear band. The regions correspond to strips of width one bubble diameter in the experiment, and 2 bubble diameters in the simulation. In order to compare numerical and experimental data, shear stress values have been scaled by the mean shear stress in the permanent regime.

$$\delta_s\sigma_i(t) = \sigma_i(t) - \overline{\sigma}(y,t) \tag{4.1}$$

where $\sigma_i(t)$ is the bubble shear stress and $\overline{\sigma}(y,t)$ is the mean shear stress in the corresponding line†. Figure 12 shows the statistical distributions of $\delta_s\sigma(i)$ (noted SSD for Static Stress Distribution), normalized by $\overline{\sigma}(y,t)$, in both the experiment and the numerical simulation. These graphs, obtained from two distinct regions of the foam, show that the SSD's are wider at the location of the shear-band than in distant regions. To quantitatively probe the evolution of this characteristics of the stress field, we monitor, for different regions of the sample, the variance of the SSD noted $\Delta_s\sigma^2$ which is defined as:

$$\Delta_s\sigma^2(t) = \frac{\sum_i a_i\ \delta_s\sigma_i^2(t)}{\sum_i a_i} \tag{4.2}$$

where a_i is the area of the bubble i. Figure 13(a) shows, in the case of the simulation, the evolution of $\Delta_s\sigma^2$ in three non-overlapping regions of the sample. A similar decrease of the three SSD's width is first observed for an imposed strain lower than 0.5. At the onset of shear-banding, the variance of the SSD significantly increases in the shear-band region (square symbols), whereas it remains constant in the rest of the material.

† the index xy are ignored in the notation of the shear stresses, but only this component is considered. The index s stands for *static* stress fluctuations, as opposed to the *dynamic* stress fluctuations studied in the next section.

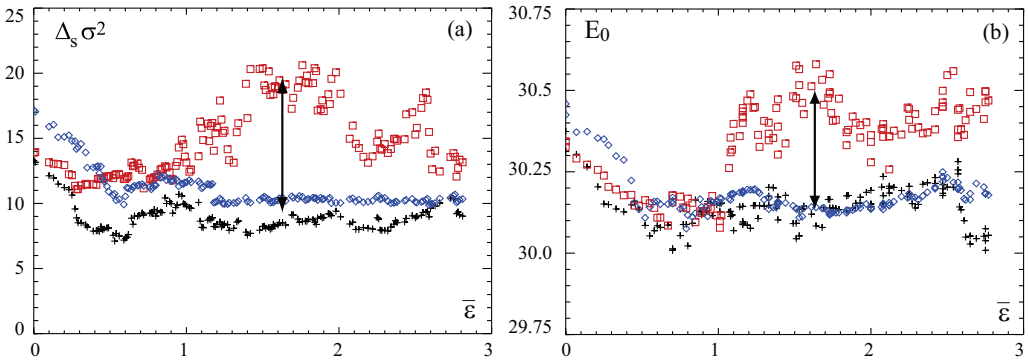

FIGURE 13. Evolution of (a) the variance $\Delta_s\sigma^2$ of the shear stress distribution (SSD) and (b) the structural energy E_0 for three different layers of the foam (simulation). The layers correspond to strips of width five bubble diameters. The squares correspond to the shear-band region, the diamonds to the neighbourhood of the opposite wall, and the cross to the middle of the foam.

Another characteristic of the foam was previously introduced, the so-called structural energy E_0, defined as the total film-length measured under zero shear stress (it is also the minimum energy of the foam for a given topology and boundary conditions). It is found to rapidly increase at the entrance of the localized regime (figure 5). Figure 13(b) shows the evolution of E_0 obtained from the three sub-regions described before. E_0 exhibits a behaviour qualitatively similar to that observed for the SSD variance.

A simple picture can clarify the physical link between these two quantities: consider a macroscopic region of the material submitted to an average shear stress $\overline{\sigma}$. Assuming that all bubbles have the same typical area a and a shear modulus μ, the energy $E(\overline{\sigma})$ of the region can be written as:

$$E(\overline{\sigma}) = \sum_i \left(e_0 + a \cdot \frac{\sigma_i^2}{2\,\mu} \right) \tag{4.3}$$

with N being the total number of bubbles, and $A = Na$ the region area. $E(\overline{\sigma})$ can also be rewritten as:

$$E(\overline{\sigma}) = Ne_0 + A\frac{\langle \delta_s \sigma_i^2 \rangle_i}{2\,\mu} + A\frac{\overline{\sigma}^2}{2\,\mu} \tag{4.4}$$

Therefore, the structural energy $E_0 = E(\overline{\sigma} = 0)$ writes, as a function of the variance of the SSD:

$$E_0 = Ne_0 + A\frac{\Delta_s\sigma^2}{2\,\mu} \tag{4.5}$$

From figure 13(a), it appears that the maximum amplitudes of variation of $\Delta_s\sigma^2$ and E_0, obtained numerically during a shear experiment, are respectively of the order of 10 and 0.4, with a subregion area $A = 0.75$. From equation 4.5, this yields an expected value for μ of the order of 10, in good agreement with the numerical measurements.

4.2. *A simple scenario for the shear-banding instability*

It has been shown that the transition to shear-banding is associated with the development of stress heterogeneities in the shear band, which can be estimated by measuring either E_0 or $\Delta\sigma^2$. As the stress distribution widens, the probability to find clusters of

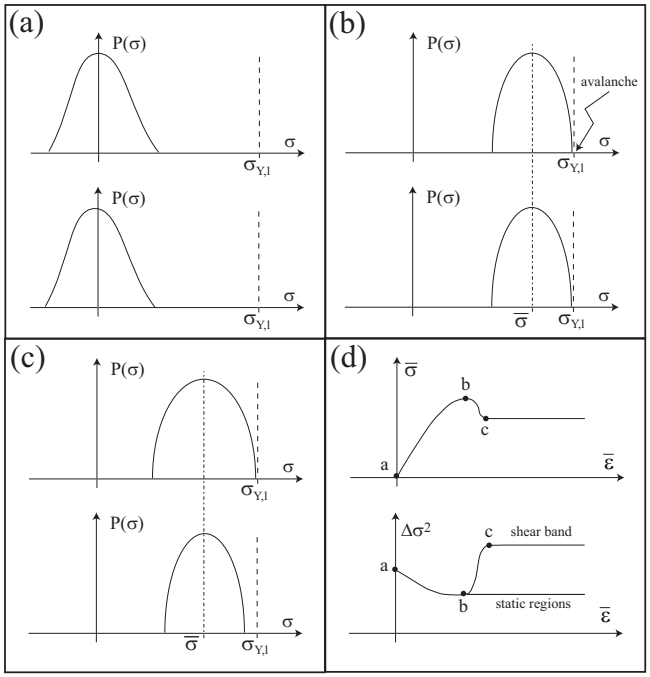

FIGURE 14. Scenario for the shear-banding instability. Figures (a), (b), and (c) show the stress distributions in two distinct regions of the foam, at three different times: (a) beginning of the experiment: the "'fresh"' foam stress field is homogeneous, (b) at the onset of shear-banding: a T1 event which triggers an avalanche of rearrangements and enlarges the stress distribution, (c) in the permanent regime: the region where the stress distribution is wider has a lower yield stress. It experiences most of the T1 events. Figure (d) displays the typical evolution of $\overline{\sigma}$, and of $\Delta\sigma^2$ in the two regions. As the shear-band develops, the yield stress decreases which results in the observed overshoot of the stress versus strain curve.

bubbles submitted to a much larger stress than the average is increased. These sites are more likely to plastically yield in response to a stress increment. It is therefore reasonable to associate the widening of the stress distribution with a decrease in the local yield stress†

Under this hypothesis, a qualitative scenario for the shear-banding instability can be proposed, based on the evolution of the local stress distributions as illustrated in Figure 14. Let us consider two distinct regions of the foam whose stress distributions are initially assumed to be similar (fig 14(a)). The initial shearing anneals a few structural defects as described in Kabla (2006). The mean shear stress increases until a large fraction of the foam is at the threshold of plastic yielding (fig 14(b)). In this critical state, a T1 event may trigger an avalanche which breaks the symmetry of the system by locally enlarging the static stress distribution, as illustrated in figure 10(a). A limited region of the foam now has a lower yield stress and is therefore more likely to experience further plastic events. This description is in many regards similar to the approach proposed by Bulatov et al. (Bulatov (1994)) in their pioneering work on disordered systems at low temperature. Interestingly, it offers a simple way to understand the overshoot of the stress versus strain relationship, observed in a wide range of systems (Khan (1988), Losert (2000)).

† Beyond this qualitative description, there is no obvious way to define a local threshold for plasticity in foams.

5. Dynamic stress fluctuations

The scenario previously described is based on the observation that plastic events induce both homogeneous stress relaxation and local stress heterogeneities. This distinction should however be refined: T1 events also produce stress heterogeneities far from their location, as depicted on figures 3 and 6. In this section, we describe in more details the dynamical properties of the stress fluctuations in the continuous flow regime induced by the successive T1 events.

5.1. *Dynamics of stress fluctuations*

We evaluate, for each bubble i, time t and time-interval Δt, the dynamic stress fluctuation (see equation 4.1):

$$\delta_d\sigma_i(t,\Delta t) = \delta_s\sigma_i(t+\Delta t) - \delta_s\sigma_i(t) \tag{5.1}$$

Figure 15 shows the resulting dynamic stress fluctuations distributions (DSFD) along with the static stress distributions (SSD), obtained from the experiment for increasing distances from the inner edge. The DSFD has been evaluated for a time interval $\Delta t = \tau_0$ corresponding to a wall displacement of one bubble diameter. Two situations can be distinguished. In the first three layers of bubbles, the SSD and the DSFD are almost identical and exhibit a remarkable gaussian shape. This similarity indicates that the static stress field is entirely renewed within a time interval smaller than τ_0. To use an analogy, the system is *thermalized* within this period of time. For increasing distances from the wheel edge, the width of the DSFD monotonically decreases and becomes significantly smaller than the width of the SSD. In these lines distant from the shear band, the stress fluctuations are insufficient to renew the frozen stress field and the system is mechanically *quenched*.

To get a more quantitative insight in the DSFD properties, its variance is measured for all time-lapses Δt and lines y:

$$\Delta_d\sigma^2(y,\Delta t) = \left\langle \delta_d\sigma_i^2(t,\Delta t)\right\rangle_{\text{bubbles within } \{y\pm\delta y\},t} \tag{5.2}$$

Figure 16(a) shows the evolution of $\Delta_d\sigma^2(y,\Delta t)$ with increasing time intervals Δt, obtained from the experiment. It exhibits a quasi-diffusive behaviour (with an exponent of the order of 0.8 for the first few lines) for $\Delta t < \tau_0$, and reaches a plateau at longer time. The transition time between these two regimes is an increasing function of the distance to the shearing edge. As shown in figure 16(b), the short time-scale diffusion constant decays exponentially with y in the vicinity of the shear band, whereas at larger distances, it exhibits a much slower decay.

5.2. *Stochastic model*

In order to understand these observations, a semi-quantitative stochastic model is developed in this section which aims to relate the T1 events statistical properties to the dynamics of stress fluctuations. For simplicity, all T1 events are assumed to produce the same stress relaxation (we thus ignore statistical deviations induced by the foam polydispersity which are found to be of the order of 30% in the simulation). We use the analytical results of Picard *et al.* (Picard (2004)) who calculated the elastic propagator associated with a discrete plastic event in a 2D elastic system, to describe the elastic perturbation induced by each T1 event. Ignoring the effect of boundaries on the stress fluctuations, the elastic propagator associated with a T1 event located at the origin thus writes, in polar coordinates (r,θ):

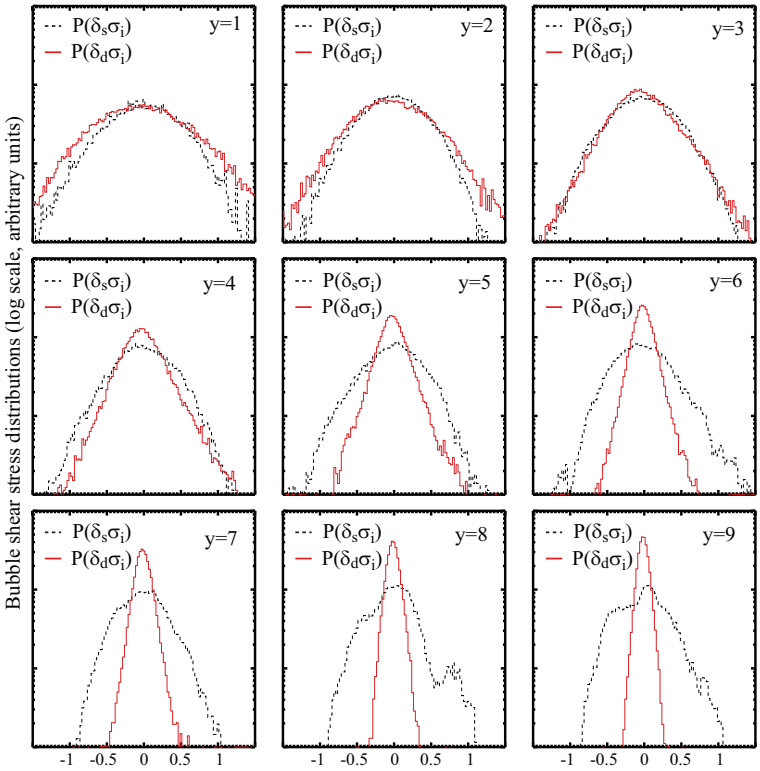

FIGURE 15. Static stress distributions $P(\delta_s\sigma_i)$ and dynamic stress distribution $P(\delta_d\sigma_i(\Delta t))$ measured in the permanent regime for $\Delta t = \tau_0$ at different distances from the inner wall. Data are obtained from the experiment during the permanent regime.

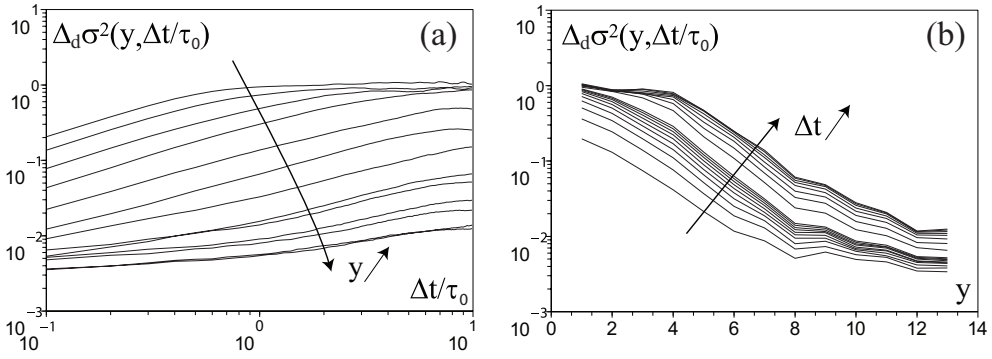

FIGURE 16. Variance of the dynamic stress fluctuations distribution (DSFD) (a) as a function of Δt for increasing distances y from the inner wheel (each curve corresponds to a line of width 1 bubble diameter), and (b) as a function of y for different $\Delta t/\tau_0$ (from 0.1 to 1, every 0.1, and from 1 to 10, every 1). These results are obtained from experimental data.

$$G(r,\theta) = \mu\delta\epsilon_{T1} + G_0(r,\theta) \quad \text{with} \quad G_0(r,\theta) = \delta\sigma_0 D^2 \cdot \frac{2\cos(4\theta)}{\pi r^2} \tag{5.3}$$

The first term in G corresponds to the homogeneous strain relaxation induced by the plastic event, whose maximum amplitude ϵ_{T1} depends on the system size (see formula (3.2)). In the fluctuation term G_0, $\delta\sigma_0$ is the stress variation associated with the lo-

cal plastic strain $\epsilon_{T_1}^{local} \sim 1$, so that $\delta\sigma_0 \sim \mu$. The functional form of G_0 exhibits the quadrupolar symmetry observed in the simulation with a $1/r^2$ decay.

5.2.1. *T1 Statistics*

In order to characterize the spatio-temporal statistics of the T1 events, we introduce the density function $f(x, y, t)$ defined as:

$$f(x, y, t) = \sum_i \delta(x - x_i)\delta(y - y_i)\delta(t - t_i) \tag{5.4}$$

where (x_i, y_i, t_i) are the coordinates in space and time of the T1 events (from this point forward, all spatial coordinates are expressed in units of bubble diameter D). It has been shown in section 3.2 that spatial correlations between rearrangements vanish after two to three T1 events. We therefore assume that T1 events appear randomly along the shear direction, which results in the following property for the T1 events density function†:

$$\langle f(x, y, t)f(x + \Delta x, y, t')\rangle_{x,t} = \tau^{-1}(y) \cdot \delta(\Delta x) \cdot \delta(t - t') \tag{5.5}$$

where $\tau^{-1}(y) = \langle f(x, y, t)\rangle_{x,t} = \partial v(y)/\partial y$ is both the line-averaged T1 frequency and the local strain-rate (formula 3.8).

The time-integrated density function $\rho(x, y, t, \Delta t) = \int_{t'=t}^{t+\Delta t} f(x, y, t')dt'$ is further introduced. This function, which measures the number of T1 events that occur between t and $t + \Delta t$ at location (x, y), may be decomposed into a mean and a fluctuating term:

$$\rho(x, y, t, \Delta t) = \tau^{-1}(y) \cdot \Delta t + \delta\rho(x, y, t, \Delta t) \tag{5.6}$$

A uniform distribution of (identical) T1 events has no effect on the shear stress fluctuations, and only leads to an homogeneous relaxation of the mean shear stress. Therefore, the stress fluctuations are controlled by the statistical properties of $\delta\rho$, which, by integration of equation 5.5 over a time Δt, is found to obey:

$$\langle \delta\rho(x, y, t, \Delta t)\delta\rho(x + \Delta x, y, t, \Delta t)\rangle_{x,t} = \tau^{-1}(y) \cdot \Delta t \cdot \delta(\Delta x) \tag{5.7}$$

In order to test the validity of this relation, the function ρ is evaluated in the simulation by monitoring, at each site (x,y) the T1 events located within a distance D/2. Figure 17(a) shows, for a line of width one bubble diameter in the shear-band, the evolution of the mean number of T1 events per site $\langle \rho(x, y, t, \Delta t)\rangle_{x,t}$ (dashed line), and the mean square deviation $\left\langle \delta\rho^2(x, y, t, \Delta t)\right\rangle_{x,t}$ (solid line) as a function of Δt. On short time-scales, $\left\langle \delta\rho^2\right\rangle_{x,t}$ and $\langle \rho\rangle_{x,t}$ exhibit a similar linear increase with Δt in agreement with formula (5.7). For $\Delta t \geq \tau(y)$ however, $\left\langle \delta\rho^2(\Delta t)\right\rangle_{x,t}$ becomes significantly smaller than $\langle \rho\rangle_{x,t}$. This second regime indicates that the hypothesis of a markovian statistics for the T1 events sequence is incorrect for integration times Δt larger than $\tau(y)$: the locations of

† This approach is formally analogous to standard stochastic descriptions of surface growth by molecules adsorption (Barabási (1995)) which allows one to describe the evolution of interface roughness as a function of the number of adsorbed molecules. Here we seek to relate the "roughness" of f, i.e. the evolution of the spatial heterogeneities in the number of T1 events per site.

the T1 events that occur between t and $t+\Delta t$ depend on the sequence of T1 events that occurred previously in a way which limit the amplitudes of variation of $\delta\rho$.

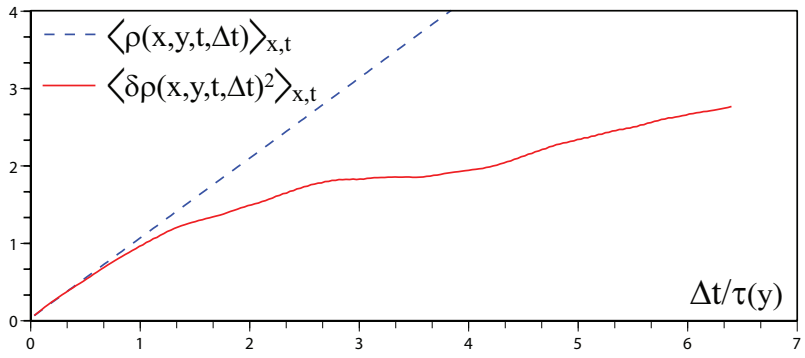

FIGURE 17. (a) Evolution of $\langle\rho(x,y,t,\Delta t)\rangle_{x,t}$ (dashed line) and $\left\langle\delta\rho(x,y,t,\Delta t)^2\right\rangle_{x,t}$ (solid line) calculated from the T1 events located within a one bubble diameter wide strip in the shear band, in permanent regime (simulation).

This effect is directly visible on figure 10(c) which shows that, in a sequence of two successive avalanches, the second one involves T1 events preferentially in the regions that have not plastically yielded during the first one. This long time-scale statistical bias can be qualitatively understood through a simple argument. If the sequence of T1 events was completely stochastic, this would lead to stress fluctuations of infinite amplitude which is incompatible with the existence of a finite yield stress. Conversely, a constraint of finite stress fluctuations would impose a bound on $\delta\rho^2$ if all rearrangements were producing the exact same stress perturbation. However, any dispersion in the values of the stress $\delta\sigma_0$, released by the T1 events, allows for a slow diffusive increase of $\delta\rho^2$ as observed in figure 17 at large Δt.

In our attempt to modelize the stress dynamics, we assumed that all the events produce a similar effect ($\delta\sigma_0$ is single valued). Consistently, $\left\langle\delta\rho^2\right\rangle$ owes to be bounded. We thus explicitely impose a maximum deviation in the total number of T1 events per site equal to 1 reached after a time $\tau(y)$ and modify the equation (5.7) accordingly:

$$\langle\delta\rho(x,y,t,\Delta t)\delta\rho(x+\Delta x,y,t,\Delta t)\rangle_{x,t} = \left(1-\exp\left(-\frac{\Delta t}{\tau(y_p)}\right)\right)\cdot\delta(\Delta x) \tag{5.8}$$

5.2.2. *Shear stress fluctuations*

Having described the statistics of the T1 events, we now seek at evaluating the stress fluctuations that they induce on a given line y. Based on equations 5.3 and 5.8, the variance of the DSFD of line y originating from T1 events taking place in line y_p can be written as:

$$\begin{aligned}\Delta_d\sigma^2_{y_p\to y}(\Delta t) &= \left\langle\left(\int_{x'}\rho(x',y,t,\Delta t)\cdot G_0(x-x',y-y_p)dx'\right)^2\right\rangle_{x,t}\\ &= \int_{X'}\int_{X''} G_0(X',y-y_p)G_0(X'',y-y_p)\\ &\qquad\langle\rho(x-X',y,t,\Delta t)\rho(x-X'',y,t,\Delta t)\rangle_{x,t}\,dX'dX''\end{aligned}$$

$$= \int_{X'} \int_{X''} G_0(X', y - y_p) G_0(X'', y - y_p) \langle \delta\rho(x - X', y, t, \Delta t) \delta\rho(x - X'', y, t, \Delta t) \rangle_{x,t} \, dX' dX''$$

$$\Delta_d \sigma^2_{y_p \to y}(\Delta t) = \frac{\delta\sigma_0^2}{\pi \cdot |y - y_p|^3} \cdot \left(1 - \exp\left(-\frac{\Delta t}{\tau(y_p)}\right)\right) \tag{5.9}$$

This relationship is only valid for $y \neq y_p$. The exact calculation for $y \sim y_p$ would require a detailed description of the plastic process at the bubble scale, which is beyond the scope of the present paper. Instead, we set the value of the elastic cut-off length at 1 (i.e. the bubble diameter) and assume that, for $r < 1$, the stress fluctuation amplitude is uniform and equal to $\delta\sigma_0$. Under this assumption, the previous developments lead to:

$$\Delta_d \sigma^2_{y_p \sim y}(\Delta t) = \delta\sigma_0^2 \cdot \left(1 - \exp\left(-\frac{\Delta t}{\tau(y_p)}\right)\right) \tag{5.10}$$

Assuming these different sources of fluctuations to be uncorrelated, the variance of the dynamic stress fluctuation distribution at a given line y can then be obtained by integrating equations 5.9 and 5.10 over y_p:

$$\Delta_d \sigma^2(y, \Delta t) = \int_{y_p} \Delta_d \sigma^2_{y_p \to y}(y, \Delta t) \, dy_p \tag{5.11}$$

5.2.3. *Numerical solutions*

This calculation yields a prediction of the statistics of the stress fluctuations in the sheared foam from the knowledge of the strain-rate profile $\tau(y)^{-1}$. In order to test this model against the experiment, we extract $\tau(y)$ from the measured plastic flow profile (figure 2). Since the latter decays exponentially with the distance from the inner wall, with a decay length of the order of one bubble diameter, $\tau(y)$ can be estimated as:

$$\tau(y) = \tau_0 \cdot \exp(y) \tag{5.12}$$

Figure 18 shows the characteristics of $\Delta_d \sigma^2(y, \Delta t)$ numerically calculated for a discrete system composed of 20 lines of bubbles ($\delta\sigma_0$ is set at 1). This model accounts for several features of its experimental counterpart (figure 16), namely (i) a diffusive regime for $\Delta t < \tau_0$, (ii) a saturation occurring after a time of order $\tau(y)$, (iii) a transition from an exponential decay in the shear-band to a power-law decay at larger distance. These two regimes can be associated with two distinct processes. Local plasticity is the main source of stress fluctuations in the layers of bubbles where a large number of T1 events occur, and the resulting stress dynamics is directly connected to the plastic frequency $\tau^{-1}(y)$ of the given line. In contrast, long-range elastic stress fluctuations induced by distant T1 events are dominant for lines with negligible plasticity†. The resulting stress fluctuations amplitude decays as a power-law with the distance to the shear-band.

5.3. *Discussion*

One of the important results of this section is that the stress fluctuations are not diffusive on long time-scales: the cumulative effect of T1 events in a given line can only produce a finite deformation of the structure in a distant line. As a result, beyond the shear-band where a large number of rearrangements are observed, these fluctuations are insufficiently intense to renew the structure (figure 15): their amplitude remains small in comparison

† This interpretation is confirmed by the experimental observation that these fluctuations exhibit large length-scale spatial correlations in distant lines, as reported in Debrégeas (2001).

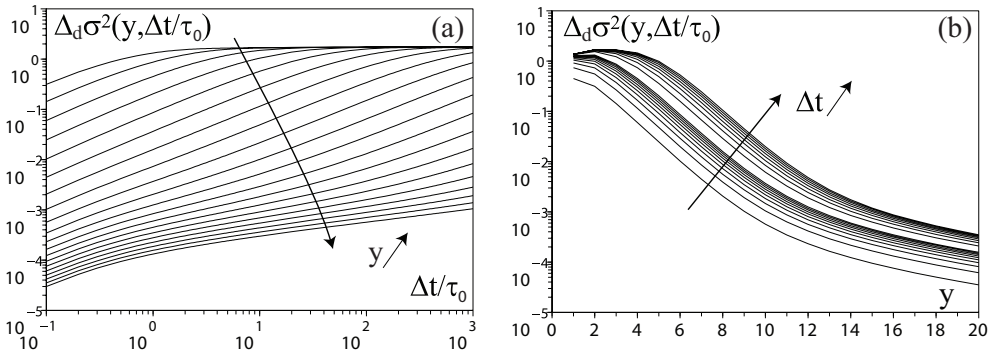

FIGURE 18. Predicted evolution of the variance of the dynamical stress fluctuations distribution (see text for details of the model). The different values for the time intervals Δt and distances y from the shearing wall, are similar to the one used in figure 16 to allow for a direct comparison with the experiment.

to the width of the static stress distribution. The latter, which is mostly set during foam preparation, thus plays a prominent role in fixing the local frequency of T1 events.

Several mean-field models of soft glasses rheology are based on empirical equations that relate the stress fluctuations amplitude to the plastic events frequency (Sollich (1997), Falk (1998)). They capture many of the features observed in foams at finite shear rate in which fluctuations originating from nearby T1 events are expected to be dominant. As mean field models, these approaches are inadequate to correctly describe the creep flow behaviour for which long-range elastic coupling becomes important. This is done in two recent numerical models which exhibit shear-banding (Baret (2002), Picard (2005)).

6. Conclusion

We showed in the companion paper that when a foam is submitted to an oscillating shear of low amplitude, the strain reduces the structural disorder by curing topological defects thus extending the elastic domain of the material. In this regime, T1 events are uncorrelated in space and time. In contrast, for large amplitude of strain, T1 events occur in the form of fracture-like processes which yield local heterogeneities in the stress field and a reduction of the yield stress. This mechanism is at the base of the shear-banding instability observed in both the simulation and the experiment.

In permanent regime, large stress fluctuations are observed even in the region where very few plastic events occur. These fluctuations are associated with the long range elastic relaxation induced by the T1 events. A simple statistical model allows one to predict the time evolution of these fluctuations from the knowledge of the time-averaged flow profile. Although the dynamic fluctuations can be estimated independently of the structure, the local T1 events frequency can not be extracted from the knowledge of the fluctuations alone. Indeed, the probability for a plastic event to occur depends on both the structural state of the system (which yields an effective yield stress), and the fluctuations that allow to reach this threshold.

Most of these results should remain valid for disordered systems at low temperature provided the existence of (1) an elastic response at low strain (2) a typical duration of plastic relaxation much shorter than the imposed shearing time-scale. The elastic propagator associated with a local plastic event will exhibit the same generic pattern, regardless of the underlying structure (Eshelby (1957), Picard (2004)), whose anisotropy

is at the origin of the fracture-like processes (see, for Lennard-Jones glasses for instance, (Maloney (2004), Shi (2005)).

The long-range elastic coupling opens the possibility for heterogeneous flows. However, the evolution toward a localized flow profile might depend on many specific characteristics of the system. Although it seems to be a robust feature in Hele-Shaw confined or 3D foams (Debrégeas (2001), Rodts (2005)), it appears to depend on preparation and geometry in granular systems for instance (Howell (1999), Mueth (2000), Fenistein (2003)). First, this effect is expected to depend on the geometrical constraints which control the way elastic stress is transmitted throughout the sample. In this respect, the dimensionality, the presence of confining walls or the shear geometry can determine the existence and stability of shear-bands. Moreover, shear-banding requires a broad enough range of disorder accessible to the system in order to allow large variations in the local yield stress. In the case of foam, this property is related, in a non-trivial way, to the foam polydispersity (Cox (2004), Wang (2006)). The precise conditions that leads to the shear-banding transition still remains to be determined.

Jean-Marc di Meglio initiated the experiments on confined foams. We wish to thank Guillemette Picard, Christiane Caroli, Olivier Pouliquen and Jean Rajchenbach for fruitful discussions. We are especially grateful to Christiane Caroli for her careful reading of the companion paper.

REFERENCES

Abd el Kader, A. & Earnshaw, J. C., 1999, Shear-Induced Changes in Two-Dimensional Foam, *Phys. Rev. Lett.* **82**, 2610–2613.

Asipauskas, M., Aubouy, M., Glazier, J. A., Graner, F. & Jiang, Y., 2003, A texture tensor to quantify deformations: the example of two-dimensional flowing foams, *Granular Matter* **5**, 71–74.

Barabási, A.-L. & Stanley, H.-E., 1995, Fractal Concepts in Surface Growth, Cambridge University Press.

Baret, J.C., Vandembroucq, D. & Roux, S., 2002, An extremal model for amorphous media plasticity, *Phys. Rev. Lett.* **89**, 195506.

Bragg, L. & Nye, J. F., 1947, A dynamical model of a crystal structure, *Proc. R. Soc. London A* **190**, 474–482.

Bulatov, V.V. & Argon A.S., 1994, A stochastic model for continuum elasto-plastic behavior: I. Numerical approach and strain localization, *Modelling Simul. Mater. Sci. Eng.* **2**, 167–184.

Bulatov, V.V. & Argon A.S. 1994 A stochastic model for continuum elasto-plastic behavior: II. A study of the glass transition and structural relaxation *Modelling Simul. Mater. Sci. Eng.* **2**, 185–202.

Bulatov, V.V. & Argon A.S. 1994 A stochastic model for continuum elasto-plastic behavior: III. Plasticity in ordered versus disordered solids *Modelling Simul. Mater. Sci. Eng.* **2**, 203–222.

Cantat, I., Kern, N. & Delannay, R., 2004, Dissipation in foam flowing through narrow channels, *Europhys. Lett.* **65**, 726–732.

Chen, K., Bak, P. & Obukhov, S.P., 1991, Self-organized criticality in a crack-propagation model of earthquakes, *Phys. Rev. A* **43**, 625.

Courty, S., Dollet, B., Elias, F., Heinig, P. & Graner, F., 2003, Two-dimensional shear modulus of a Langmuir foam, *Europhys. Lett* **64**, 709–715.

Cox, S., Weaire, D. & Glazier, J.A., 2004, The rheology of two-dimensional foams, *Rheol Acta* **43**, 442–448.

Debrégeas, G., Tabuteau, H. & di Meglio, J.-M., 2001, Deformation and flow of a Two-Dimensional Foam under Continuous Shear, *Phys. Rev. Lett.* **87**, 178305.

Dennin, M. & Knobler C. M., 1997, Experimental Studies of Bubble Dynamics in a Slowly Driven Monolayer Foam, *Phys. Rev. Lett.* **78**, 2485–2488.

Dollet, B., Elias, F., Quilliet, C., Raufaste, C., Aubouy, M. & Graner, F., 2005, Two-dimensional flow of foam around an obstacle: Force measurements, *Phys. Rev. E* **71**, 031403.

Durian, D. J., Weitz, D. A. & Pine, D. J., 1991, Multiple light-scattering probes of foam structure and dynamics, *Science* **252**, 686-688.

Eshelby, J.D., 1957, The determination of the elastic field of an ellipsoidal inclusion and related problems, *Proc. R. Soc. London, Ser. A* **241**, 376.

Falk, M.L. & Langer, J.S., 1998, Dynamics of viscoplastic deformation in amorphous solids, *Phys. Rev. E* **57**, 7192.

Fenistein, D. & van Hecke, M., 2003, Wide shear zones in granular bulk flow, *Nature* **425**, 256.

Hohler, R., Cohen-Addad, S. & Hoballah, H., 1997, Periodic Nonlinear Bubble Motion in Aqueous Foam under Oscillating Shear Strain, *Phys. Rev. Lett.* **79**, 1154–1157.

Howell, D., Behringer, R.P. & Veje, C., 1999, Stress Fluctuations in a 2D Granular Couette Experiment: A Continuous Transition, *Phys. Rev. Lett.* **82**, 5241–5244.

Kabla, A. & Debrégeas, G., 2003, Local stress relaxation and shear-banding in a dry foam under shear, *Phys. Rev. Lett.* **90**, 258303.

Kabla, A. & Debrégeas, G., 2006, Quasistatic Rheology of Foam: I. Low Deformation Response, *submitted*.

Khan, S. A., Schnepper, C. A. & Armstrong, R. C., 1988, Foam rheology: III Measurement of shear flow properties, *Journal of Rheology* **32**, 69–92.

Kraynik, A.M., Reinelt, D.A. & van Swol, F., 2003, Structure of random monodisperse foam, *Phys. Rev. E* **67**, 031403.

Lauridsen, J., Twardos, M. & Dennin, M., 2002 Shear-Induced Stress Relaxation in a Two-Dimensional Wet Foam, *Phys. Rev. Lett.* **89**, 098303.

Maloney, C. & Lemaitre, A., 2004, Subextensive Scaling in the Athermal, Quasistatic Limit of Amorphous Matter in Plastic Shear Flow, *Phys. Rev. Lett.* **93**, 016001.

Losert, W., Géminard, J.-C., Nasuno, S. & Gollub, J.P., 2000, Mechanisms for slow strengthening in granular materials, *Phys. Rev. E* **61**, 4060–4068.

Mueth, D.M., Debregeas, G., Karczmar, G.S., Eng, P.J., Nagel, S.R. & Jaeger, H.M., 2000, Signaturesofgranularmicrostructure in dense shear flows, *Nature* **406**, 385–389.

Okuzono, T. & Kawasaki, 1995, Intermittent flow behavior of random foams: a computer experiment on foam rheology, *Phys. Rev. E* **1995**, 1246–1253.

Picard, G., Ajdari, A., Lequeux, F. & Bocquet L., 2004, Elastic consequences of a single plastic event: A step towards the microscopic modeling of the flow of yield stress fluids., *Eur. Phys. J. E.* **15**, 371–381.

Picard, G., Ajdari, A., Lequeux, F. & Bocquet L., 2005, Slow flows of yield stress fluids: Complex spatiotemporal behavior within a simple elastoplastic model, *Phys. Rev. E* **71**, 010501(R).

Pratt, E. & Dennin, M., 2003, Nonlinear stress and fluctuation dynamics of sheared disordered wet foam, *Phys. Rev. E* **67**, 051402.

Rodts, S., Baudez, J. C. & Coussot, P., 2005, From discrete to continuum flow in foams, *Europhys. Lett.* **69**, 636–642.

Shi, Y. & Falk, M.L., 2005, Strain Localization and Percolation of Stable Structure in Amorphous Solids, *Phys. Rev. Lett.* **95**, 095502.

Sollich, P., Lequeux, F., Hébraud, P. & Cates, M.E., 1997, Rheology of soft glassy materials, *Phys. Rev. Lett.* **78**, 2020.

Varnik, F., Bocquet, L., Barrat, J.-L. & Berthier, L., 2003, Shear Localization in a Model Glass, *Phys. Rev. Lett.* **90**, 095702.

Wang, Y., Krishan, K. & Dennin, M., 2006, Impact of boundaries on the velocity profiles in bubble rafts, *Phys. Rev. E* **73**, 031401.

Weaire, D. & Kermode, J.P., 1983, Computer simulation of a two-dimensional soap froth I. Method and motivation, *Philosophical Magazine B* **48**, 245–259.

Weaire, D. & Hutzler, S., 1999, The Physics of Foams, Clarendon Press, Oxford.